


**Numerical simulation of knotted solutions for Maxwell equations**Antonio M. Valverde , Luis D. Angulo , M. R. Cabello, and Salvador G. García *Department of Electromagnetism, University of Granada, Granada 18071, Spain*Juan J. Omiste *Instituto Madrileño de Estudios Avanzados en Nanociencia (IMDEA-Nanociencia), Cantoblanco, Madrid 28049, Spain  
and Departamento de Química, Universidad Autónoma de Madrid, Módulo 13, Madrid 28049, Spain*

Jianshu Luo

*National University of Defense Technology, 137 Yanwachi, Changsha, Hunan 410073, People's Republic of China*

(Received 4 February 2020; accepted 12 April 2020; published 8 June 2020)

In this work, we use the finite differences in time domain (FDTD) numerical method to compute and assess the validity of Hopf solutions, or hopfions, for the electromagnetic field equations. In these solutions, field lines form closed loops characterized by different knot topologies which are preserved during their time evolution. Hopfions have been studied extensively in the past from an analytical perspective but never, to the best of our knowledge, from a numerical approach. The implementation and validation of this technique eases the study of more complex cases of this phenomena; e.g., how these fields could interact with materials (e.g., anisotropic or nonlinear), their coupling with other physical systems (e.g., plasmas), and also opens the path on their artificial generation by different means (e.g., antenna arrays or lasers).

DOI: [10.1103/PhysRevE.101.063305](https://doi.org/10.1103/PhysRevE.101.063305)**I. INTRODUCTION**

Hopfions are a family of localized solutions for the electromagnetic field Maxwell equations in which field lines are closed, forming knotted topologies which are preserved when evolved in time [1–3]. Beyond their intrinsic mathematical interest, these solutions may also contribute to several branches of physics. Some authors have proposed that they play a key role in the phenomena known as *ball lightning* [4,5] or as exotic quantum mechanical solutions that describe the electron at a fundamental level, predicting some of its properties [6–8].

In the past, hopfions have been studied exclusively from an analytical perspective [1,9–15]. However, to the best of our knowledge, they have never been simulated numerically. These simulations can be of interest for several reasons: first, because hopfions are demonstrated to exist, not only from purely analytical arguments, but from the direct numerical resolution of the elemental Maxwell's curl equations. Additionally, a validated numerical approach opens many possibilities to study more complicated variants of these phenomena, e.g., the study of their interactions with anisotropic or nonlinear materials, with other hopfions [16], their coupling with other physical equations, or the possibility of generating them by means of antenna arrays or lasers; a technique which was proposed as a way for their physical realization but has not been accomplished yet [1].

The accuracy assessment of hopfion numerical solutions is a necessary step to address certain physical problems which are not feasible analytically. To this end, in this work we use the finite-difference time-domain (FDTD) method [17,18], a proven and robust method which is ubiquitous in computational electrodynamics, and which is possibly the optimal approach given the spatial and time scales involved. The input of

the method is an initial known analytical hopfion solution and the obtained numerical evolution results are then compared with the expected analytical solution. Different metrics are proposed as tools to assess the validity of this approach.

This work is organized as follows: first, in Sec. II we give a theoretical background, focusing on the construction of hopfions and their helicity conservation property. Second, we briefly describe the FDTD method. Next, in Sec. III we describe the propagation of the hopfion based on the numerical simulations as well as the conservation of the helicity as a benchmark. In this context, we also introduce a metric to quantify the error in the propagation. Finally, in Sec. IV we summarize the main conclusion of this study along with possible extensions and applications.

**II. BACKGROUND****A. Theory**

Hopfions were proposed in 1989 by Rañada [11]. In that work, he formulated a particular solution for Maxwell's equation in which all field lines are closed and form a torus which deforms over time while, at the same time, preserving its topology. This result was then extended and categorized as part of a family of solutions characterized by an arbitrary number of mathematical *knots*, i.e., embeddings of a circle in a three-dimensional Euclidean space [1,12]. In this regard, Rañada's torus has a circumferential core which within this family of solutions corresponds to the knot known as *the unknot*. However, with the exception of Rañada's hopfion, these generalized hopfion topologies did not preserve over time. In 2013 Kedia *et al.* [10] brought to light an analytical construction which allows us to formulate a whole family of

knotted solutions for Maxwell's equations, where Rañada's torus is a particular case.

It is widely accepted that light knots must be null fields as a necessary condition to preserve helicity [10,19], whereas only hopfions preserve the topology at every time [13,20,21]. The properties of the null fields are

(1) Electric and magnetic fields are perpendicular at every point:  $\mathbf{E} \perp \mathbf{B}$ .

(2) They have the same magnitude:  $|\mathbf{E}| = |\mathbf{B}|$ .

Assuming this hypothesis, we may apply *Bateman's method* to build null fields. First, we define the Riemann-Silberstein vector  $\mathbf{F}$ ,

$$\mathbf{F} = \mathbf{E} + i\mathbf{B}, \quad (1)$$

where  $\mathbf{B}$  and  $\mathbf{E}$  represent the magnetic and electric fields, respectively. Note that we use the electromagnetic natural units in which the vacuum electric permittivity, magnetic permeability, and speed of light ( $\epsilon_0$ ,  $\mu_0$ , and  $c$ , respectively) are equal to 1.

Bateman's method proves that every Riemann-Silberstein vector corresponding to a null field can be written as

$$\mathbf{F} = \nabla\alpha \times \nabla\beta \quad (2)$$

where  $\alpha$  and  $\beta$  can be any complex functions as long as they meet the following condition:

$$\nabla\alpha \times \nabla\beta = i \left( \frac{\partial\alpha}{\partial t} \nabla\beta - \frac{\partial\beta}{\partial t} \nabla\alpha \right). \quad (3)$$

Kedia *et al.* [10] found these specific expressions for  $\alpha$  and  $\beta$ :

$$\alpha = \left( \frac{r^2 - t^2 - 1 + 2iz}{r^2 - (t - i)^2} \right)^p, \quad (4)$$

$$\beta = \left( \frac{2(x - iy)}{r^2 - (t - i)^2} \right)^q, \quad (5)$$

where  $p$  and  $q$  must be positive coprime integers which lead us to different kinds of knots. Note that the expressions (4) and (5) have been obtained assuming an arbitrary distance ( $l_0$ ) and time ( $t_0 = l_0/c$ ) units which set the hopfion scale.

The knotness of a hopfion can be characterized by its *magnetic* and *electrical helicities*,  $h_B$  and  $h_E$  respectively [1,22], defined as

$$h_B(\mathbf{B}) = \int_D \mathbf{A} \cdot \mathbf{B} d^3\mathbf{r}, \quad h_E(\mathbf{E}) = \int_D \mathbf{C} \cdot \mathbf{E} d^3\mathbf{r}, \quad (6)$$

where  $\mathbf{B} = \nabla \times \mathbf{A}$ ,  $\mathbf{E} = \nabla \times \mathbf{C}$ , and  $D$  represents the domain. Note that as the helicity is a measurable quantity, it must be gauge independent.

Let us prove that the magnetic helicity is invariant under gauge transformations, i.e., the magnetic helicity for  $\mathbf{A} + \nabla f$ , noted as  $\bar{h}_B(\mathbf{B})$ , is equal to  $h_B(\mathbf{B})$ . We compute  $\bar{h}_B(\mathbf{B})$  using Eq. (6):

$$\begin{aligned} \bar{h}_B(\mathbf{B}) &= \int_D (\mathbf{A} + \nabla f) \cdot \mathbf{B} d^3\mathbf{r} = h_B(\mathbf{B}) + \int_D \nabla f \cdot \mathbf{B} d^3\mathbf{r} \\ &= h_B(\mathbf{B}) + \int_D \nabla \cdot (f\mathbf{B}) d^3\mathbf{r} - \int_D f \nabla \cdot \mathbf{B} d^3\mathbf{r} \\ &= h_B(\mathbf{B}) + \int_{\partial D} f \cdot \mathbf{B} dS = h_B(\mathbf{B}), \end{aligned} \quad (7)$$

where we have used  $\nabla \cdot \mathbf{B} = 0$  and imposed the condition that the magnetic field vanishes in the boundary of  $D$ , i.e.,  $\mathbf{B}|_{\partial D} = 0$ . Using a similar procedure, we obtain the result that the helicity of the electric field is also preserved.

Now, we prove that  $h_B$  and  $h_E$  do not change in time for null fields. The time derivative of the magnetic helicity is

$$\begin{aligned} \partial_t h_B(\mathbf{B}) &= \int_D \partial_t \mathbf{A} \mathbf{B} d^3\mathbf{r} + \int_D \mathbf{A} \partial_t \mathbf{B} d^3\mathbf{r} \\ &= - \int_D \mathbf{E} \cdot \mathbf{B} d^3\mathbf{r} + \int_D \mathbf{A} \nabla \times \partial_t \mathbf{A} d^3\mathbf{r}, \end{aligned} \quad (8)$$

then, we use [23]

$$\nabla(\mathbf{U} \times \mathbf{V}) = (\nabla \times \mathbf{U}) \cdot \mathbf{V} - (\nabla \times \mathbf{V}) \cdot \mathbf{U} \quad (9)$$

and we set  $\mathbf{U} = \mathbf{A}$  and  $\mathbf{V} = \partial_t \mathbf{A}$ . Thus, Eq. (8) reads as

$$\begin{aligned} \partial_t h_B(\mathbf{B}) &= - \int_D \mathbf{E} \cdot \mathbf{B} d^3\mathbf{r} - \int_D \nabla(\mathbf{A} \times \partial_t \mathbf{A}) d^3\mathbf{r} \\ &\quad + \int_D \partial_t \mathbf{A} \nabla \times \mathbf{A} d^3\mathbf{r} \\ &= -2 \int_D \mathbf{E} \cdot \mathbf{B} d^3\mathbf{r} - \int_{\partial D} \mathbf{A} \times \partial_t \mathbf{A} dS = 0, \end{aligned} \quad (10)$$

where we have used the conditions that the null fields fulfill  $\mathbf{E} \cdot \mathbf{B} = 0$ , that  $\partial_t \mathbf{A} = -\mathbf{E} - \nabla\varphi$  vanishes in the boundary  $\partial D$  and  $\int_D \mathbf{B} \nabla\varphi d^3\mathbf{r} = \int_D \nabla(\varphi\mathbf{B}) d^3\mathbf{r} - \int_D \varphi \nabla\mathbf{B} d^3\mathbf{r} = 0$ . Using a similar procedure we can prove that the electric helicity is constant over time.

## B. The finite differences in time domain method

The Yee FDTD scheme [17] numerically solves Maxwell curl equations by replacing the space and time derivatives by finite differences. Any unknown field component can be advanced a time step using the ones at adjacent space positions. To obtain an optimized algorithm, fields are arranged strategically on the center of the edges and faces of a cubic cell of size  $\Delta$ ; a configuration known as Yee's cell [17]. For instance, to evolve the  $E_z$  component a time step  $\Delta t$  we obtain the following formula in free-space:

$$\begin{aligned} E_z|_{\bar{i},\bar{j},k}^{\bar{n}} &= E_z|_{\bar{i},\bar{j},k}^{\bar{n}-1} + \frac{\Delta t}{\Delta} (H_y|_{i,\bar{j},k}^n - H_y|_{i+1,\bar{j},k}^n \\ &\quad - H_x|_{\bar{i},j,k}^n + H_x|_{\bar{i},j+1,k}^n), \end{aligned} \quad (11)$$

where  $i, j, k$  are integer numbers identifying each cell and time step at a time step  $n$ ; barred indices indicate the addition of a half step, e.g.,  $\bar{i} = i + 1/2$ , and  $B = \mu H$ . For problems solved in free space, like the ones addressed in this paper, this scheme is demonstrated to have second-order error convergence with respect to a  $\Delta$  refinement [18]; i.e., the numerical error decays as  $O(\Delta^2)$ .

In order to compute a simulation, Maxwell's equations are propagated inside a finite box endowed with boundary conditions. As our aim is to simulate a hopfion which is assumed to be isolated in an infinite space, we must set transparent boundary conditions absorbing all the energy exiting the domain. The most widely used ones in FDTD, for this purpose, are those of Berenger's perfectly matched layer (PML) method [24].

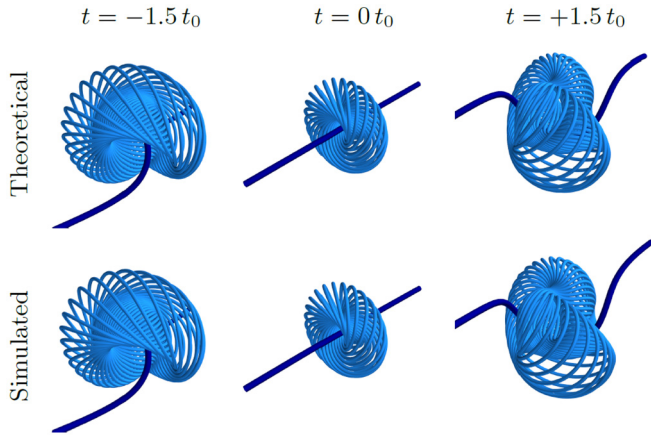


FIG. 1. Analytical (first row) and computed (second row) electric field lines for hopfion {1,1}. Dark lines correspond to the only field line that does not close on itself.

The PML method employs a nonphysical reflectionless anisotropic medium [25] surrounding the physical one, with an impedance matched to that of the surrounded medium for all angles of incidence and all frequencies.

The numerical PML is implemented as a finite-thickness slab, backed by perfect electrically conducting conditions. The conductivity  $\sigma$  inside it is usually taken with a polynomial growth away from the physical-PML interface, according to

$$\sigma(d) = \left(\frac{d}{l}\right)^m \sigma_{\max}, \quad (12)$$

with  $d$  being the distance from the interface and  $l$  the PML thickness. The PML slab is demonstrated [18] to present a normal arbitrarily small reflection coefficient  $R_0$ , from which  $\sigma_{\max}$  is found in turn by

$$\sigma_{\max} = -\frac{(m+1) \log_{10}(R_0)}{2l}. \quad (13)$$

All the cases described in this work were performed using  $m = 2$ ,  $R_0 = 0.001$ , and ten FDTD cells of PML, each one with the same spatial increment used for the interior medium,  $\Delta = 0.025$  ( $l = 10\Delta$ ).

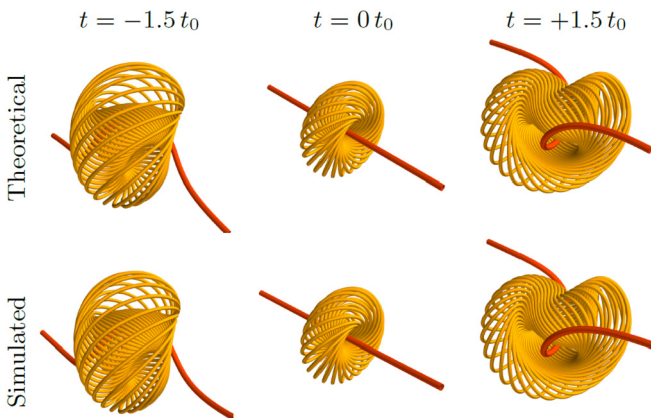


FIG. 2. For hopfion {1,1}, analytical (first row) and computed (second row) magnetic field lines. Dark lines correspond to the only field line that does not close on itself.

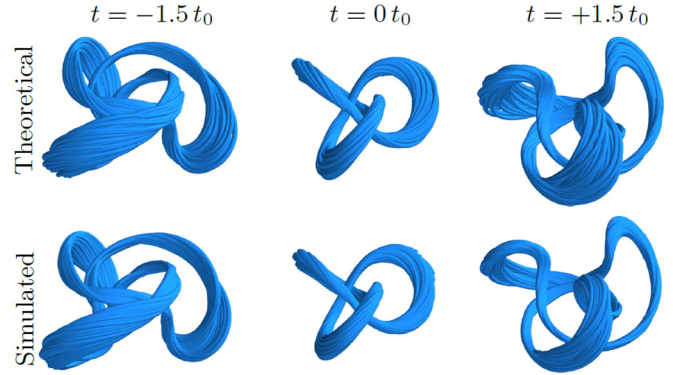


FIG. 3. For hopfion {2,3}, analytical (first row) and computed (second row) electric field lines.

### III. RESULTS AND VALIDATION

In this section, we study the time propagation of the numerical hopfion solutions, cross-validated with analytical results. The time-domain nature of the FDTD method allows us to visualize different snapshots of the time evolution. The initial time step is set to  $t = -1.5t_0$ , the computational domain is a cubic box of  $17.5l_0 \times 17.5l_0 \times 17.5l_0$ , with a spatial step  $\Delta = 0.025 l_0$  and a temporal step of  $\Delta t = 0.8\Delta/\sqrt{3}$ . All the results shown in this work were obtained using an Intel(R) Core(TM) i7-4710MQ personal computer with 16 GB of RAM. We focus our discussion on two types of hopfions obtained by setting  $\{p = 1, q = 1\}$  and  $\{p = 2, q = 3\}$  in expressions (4) and (5).

#### A. Hopfion's dynamics

First, we analyze the hopfion {1,1}, also known as Rañada's torus or the unknot. In Figs. 1 and 2 we show the analytical and numerically computed electric and magnetic field lines, respectively, at three different times. Let us remark that the toruslike shapes of field lines are similar for the electric and magnetic fields. Furthermore, the computational results reproduce very accurately the analytical ones, and are indistinguishable in the scale of the figure. On the other hand, in Figs. 3 and 4 we show the analytical and computed hopfion {2,3} solution for the electric and magnetic fields as a function of time. As in the previous case, its topology structure, i.e., the trefoil knot, is preserved during the time propagation. However, we see that the field lines of the simulated hopfion at

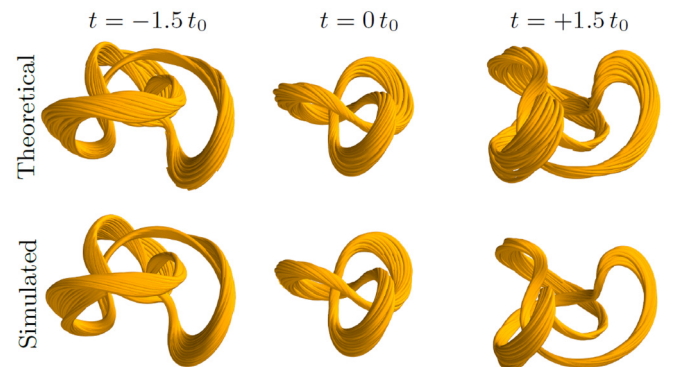


FIG. 4. For hopfion {2,3}, analytical (first row) and computed (second row) magnetic field lines.

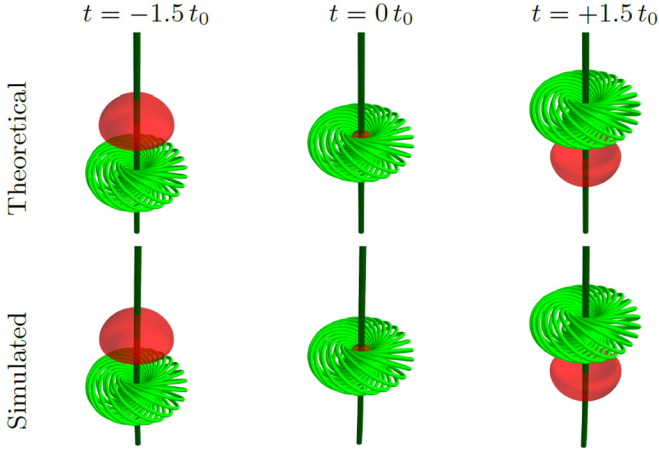


FIG. 5. For hopfion  $\{1,1\}$ , analytical (first row) and computed (second row) Poynting field lines. Dark lines correspond to the only field line that does not close on itself. Red surfaces correspond to an area in which the Poynting vector has a constant magnitude (half of its maximum value).

$t = 1.5t_0$  are closer than in the theoretical simulation; i.e., this simulation tends to stick to the field lines. This error occurs because of the complexity of hopfion  $\{2,3\}$ , whose structure is more tangled than hopfion  $\{1,1\}$ . However, this error can be suppressed by using a more dense computational grid. Even so, this error is not remarkable, as we will discuss in more detail in Sec. III B.

In Figs. 5 and 6 we shown Poynting vector field lines for hopfions  $\{1,1\}$  and  $\{2,3\}$ , respectively. Interestingly, in both cases we can appreciate that they correspond to the *unknot*, even for hopfion  $\{2,3\}$ , whose electric and magnetic fields correspond to the *trefoil knot*. Moreover, for both hopfions we may note that the torus defined by the Poynting vector field moves from bottom to top of the Z axis without deformation while the electromagnetic energy moves from top to bottom. The main difference we appreciate is the energy distribution. If we now compare the simulated and theoretical results we may see that they are virtually identical, even considering that interpolations of the simulation results were necessary to obtain these field lines.

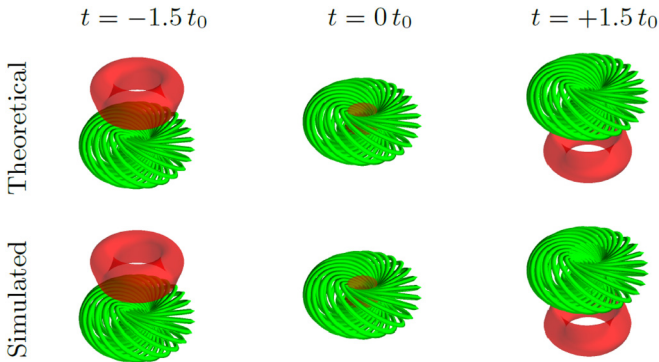


FIG. 6. For hopfion  $\{2,3\}$ , analytical (first row) and computed (second row) Poynting field lines. Red surfaces correspond to an area in which the Poynting vector has a constant magnitude (half of its maximum value).

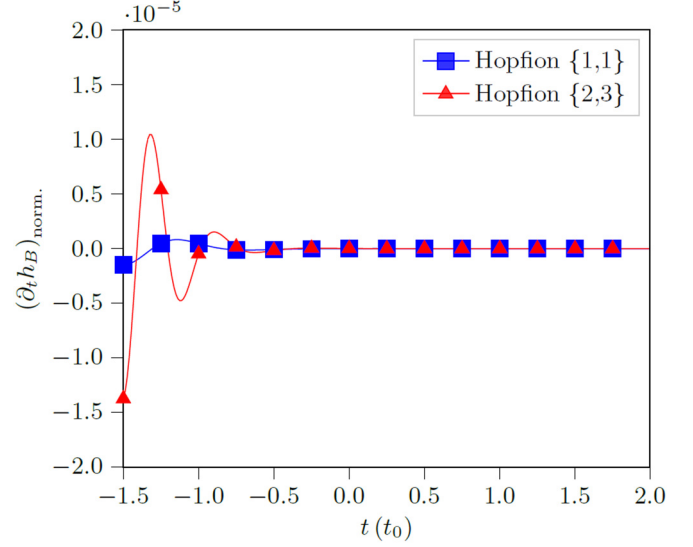


FIG. 7. Representation of normalized  $\partial_t h_B$  over time for hopfions  $\{1,1\}$  and  $\{2,3\}$ .

At first glance, the knotness is conserved during the numerical propagation, as in the theoretical solution. In order to quantify the conservation of knotness, we now investigate the helicity, which is related to the topology of the solution, since it only takes a nonzero value if the topology of the magnetic (electric) field lines are not trivial [8]. In particular we analyze the time propagation of the magnetic helicity,  $h_B$ , without loss of generality, since the results are equivalent for  $h_E$ . To do so, we define the normalized derivative of  $h_B$  as

$$(\partial_t h_B)_{\text{norm.}} = \frac{\partial_t h_B}{\int_D |\mathbf{E}| \cdot |\mathbf{B}| d^3\mathbf{r}}. \quad (14)$$

As we have proved in Eq. (10), the helicity associated with the magnetic and electric fields is a conserved quantity in a hopfion, thus, we expect that  $(\partial_t h_B)_{\text{norm.}} = 0$  during the propagation.

In order to validate our method, we plot  $(\partial_t h_B)_{\text{norm.}}$  as a function of time in Fig. 7. Note that we compute  $(\partial_t h_B)_{\text{norm.}}$  for an inset with a side of  $10l_0$  centered in the computational domain. For both cases we find that  $(\partial_t h_B)_{\text{norm.}}$  at  $t = -1.5t_0$  is slightly different from zero and continues oscillating before converging to zero exponentially. This behavior at initial times is associated with modes unsupported by FDTD, caused by the discretization of the analytical hopfion used as the initial condition. However, these modes do not play a role in long term dynamics as FDTD makes  $(\partial_t h_B)_{\text{norm.}}$  converge to zero after a few oscillations. This process takes around  $2t_0$ , which is a short interval compared to the temporal scale associated with the size of the simulation box.

## B. Error propagation

In this section, we use the following metric to assess the numerical error of our methodology:

$$\text{Err}(U)_{i,j,k}^n = \left| \frac{U_{\text{theor}}^n|_{i,j,k} - U_{\text{sim}}^n|_{i,j,k}}{U_{\text{theor}}^n|_{i,j,k}} \right|, \quad (15)$$

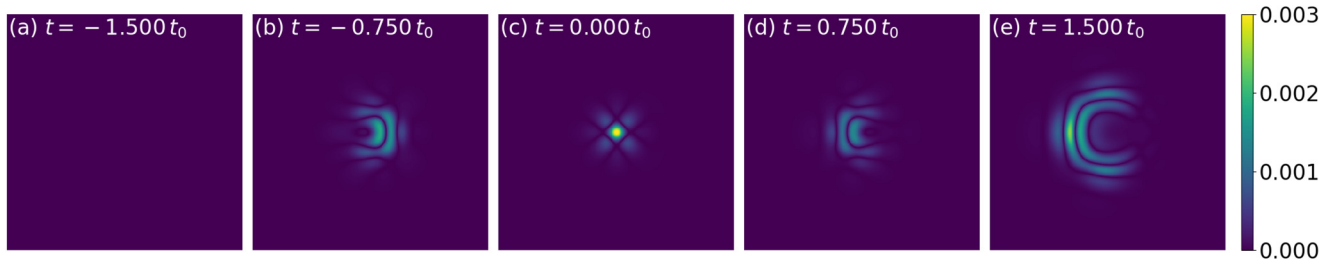


FIG. 8. For the hopfion {1, 1}, simulation error of the  $E_y$  component at the cross section  $Y = 0$ .

where  $U$  corresponds to a field,  $i, j, k$  to a point in the grid, and  $n$  to the  $n$ th time step.

In Figs. 8 and 9, we show  $\text{Err}(U)|_{i,j,k}^n$  on the plane  $Y = 0$  for the  $y$  component of  $\mathbf{E}$  for the hopfions {1, 1} and {2, 3}, respectively. Note that we represent the error only for one vector component in order to avoid any numerical artifact which could be caused by the interpolation necessary due to the staggered nature of the FDTD algorithm. This metric evaluates the relative error with respect to the theoretical value of each component at every point, which allows us to obtain the percentage error. This is expected to be higher where the theoretical value is zero. In these points, the most tiny differences can cause the relative error to go up to infinity. For visualization purposes, we have chosen to show the numerical error for a component in which the theoretical value is never zero, this being  $E_y$  at plane  $Y = 0$ . The figures correspond to an inset of  $10l_0$  from a computational domain of  $17.5l_0$ .

First of all, we realize that the error for hopfion {1,1} is smaller than for hopfion {2,3}, which can be attributed to the numerical dispersion due to the higher spatial and temporal variations of the latter solution. We observe that the error propagates in every direction, being negligible at  $t = -1.5t_0$  since it corresponds to the first iteration. After that, the error increases, spreading around the center of the grid, as we see for instance in Fig. 8(b). At  $t = 1.5t_0$  the error is less than 2% for hopfion {2,3} and even lower for hopfion {1,1}, with a maximum value of 0.3%.

The numerical dispersion error has no impact on the helicity, a basic property of hopfions, which demonstrates the suitability of the FDTD to propagate this type of solution. Specifically, the FDTD preserves the component  $\mathbf{E} \cdot \mathbf{B}$  by construction, making it an ideal method to simulate null fields, as in the present case.

IV. CONCLUSIONS AND OUTLOOK

We have demonstrated that FDTD is a viable alternative to simulate different kinds of light knots. Specifically, taking hopfion {1,1} as a benchmark, we have shown that the FDTD is an efficient and accurate method to propagate this solution of Maxwell’s equation. Using the same grid we have reproduced accurately the dynamics of a more tangled hopfion, in particular hopfion {2,3}, which shows that FDTD is suitable to simulate this kind of structure. Besides, we have shown that the helicity variation converges to zero in a short time, which is a proof that the topology is preserved during the propagation. Furthermore, it is important to note that the FDTD method would allow for improved results, if necessary, by using a finer discretization.

This work opens new lines of investigation, since it paves the way to investigate the hopfions beyond the analytical expressions (4) and (5), which are too complex to solve analytically in many physical systems. For example, the FDTD will allow us to investigate their generation and confinement as well as the interaction of hopfions among them or with other structures such as metal, metamaterials or plasma, among many others. Moreover, the numerical simulations can be used to design experimental setups to produce hopfions in the laboratory. Such experiments are of great interest, since they may measure ball lightning, which has been hypothesized to be hopfions or hopfions linked to plasma.

ACKNOWLEDGMENTS

The work described in this paper and the research leading to these results have been supported by the Spanish MINECO and EU FEDER under Project No. TEC2016-79214-C3-3-R (MINECO, Spain). J.J.O. also acknowledges support from the FULMATEN-CM (Ref. Y2018/NMT-5028) funded by the Programme of R&D Activities of Comunidad de Madrid (Spain) and the Social European Fund.

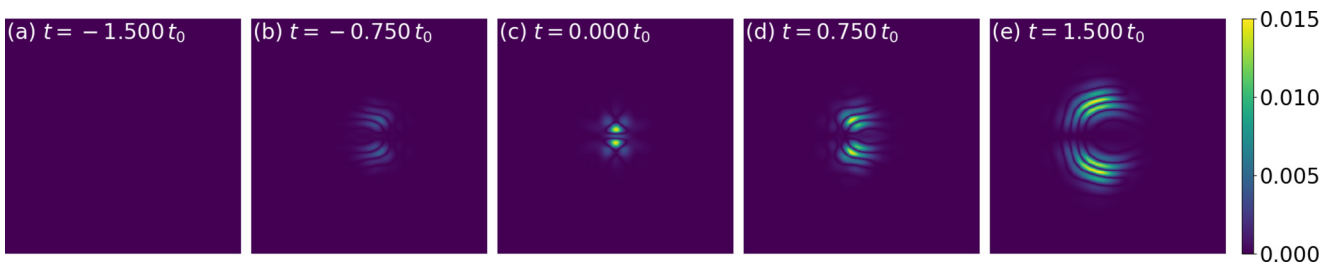


FIG. 9. For the hopfion {2, 3}, simulation error of the  $E_y$  component at the cross section  $Y = 0$ .

- [1] W. T. M. Irvine and D. Bouwmeester, Linked and knotted beams of light, *Nat. Phys.* **4**, 716 (2008).
- [2] O. Lechtenfeld and G. Zhilin, A new construction of rational electromagnetic knots, *Phys. Lett. A* **382**, 1528 (2018).
- [3] R. P. Cameron, Monochromatic knots and other unusual electromagnetic disturbances: Light localised in 3D, *J. Phys. Commun.* **2**, 15024 (2018).
- [4] A. F. Rañada and J. L. Trueba, Ball lightning an electromagnetic knot? *Nature (London)* **383**, 32 (1996).
- [5] A. F. Rañada, M. Soler, and J. L. Trueba, Ball lightning as a force-free magnetic knot, *Phys. Rev. E* **62**, 7181 (2000).
- [6] W. Lee, A. H. Gheorghe, K. Tiurev, T. Ollikainen, M. Möttönen, and D. S. Hall, Synthetic electromagnetic knot in a three-dimensional skyrmion, *Sci. Adv.* **4** eaao3820 (2018).
- [7] A. F. Rañada and J. L. Trueba, A topological mechanism of discretization for the electric charge, *Phys. Lett. B* **422**, 196 (1998).
- [8] A. F. Rañada, Topological electromagnetism, *J. Phys. A: Math. Gen.* **25**, 1621 (1992).
- [9] W. T. M. Irvine, Linked and knotted beams of light, conservation of helicity and the flow of null electromagnetic fields, *J. Phys. A: Math. Theor.* **43**, 385203 (2010).
- [10] H. Kedia, I. Bialynicki-Birula, D. Peralta-Salas, and W. T. M. Irvine, Tying Knots in Light Fields, *Phys. Rev. Lett.* **111**, 150404 (2013).
- [11] A. F. Rañada, A topological theory of the electromagnetic field, *Lett. Math. Phys.* **18**, 97 (1989).
- [12] Y. Kawaguchi, M. Nitta, and M. Ueda, Knots in a Spinor Bose-Einstein Condensate, *Phys. Rev. Lett.* **100**, 180403 (2008).
- [13] M. Arrayás and J. L. Trueba, A class of non-null toroidal electromagnetic fields and its relation to the model of electromagnetic knots, *J. Phys. A: Math. Theor.* **48**, 025203 (2015).
- [14] M. Arrayás and J. L. Trueba, Torus-knotted electromagnetic fields, [arXiv:1106.1122](https://arxiv.org/abs/1106.1122).
- [15] M. Arrayás and J. L. Trueba, On the fibration defined by the field lines of a knotted class of electromagnetic fields at a particular time, *Symmetry* **9**, 218 (2017).
- [16] M. Arrayás and J. L. Trueba, Collision of two hopfions, *J. Phys. A: Math. Theor.* **50**, 085203 (2017).
- [17] K. Yee, Numerical solution of initial boundary value problems involving Maxwell's equations in isotropic media, *IEEE Trans. Antennas Propag.* **14**, 302 (1966).
- [18] A. Taflov and S. C. Hagness, *Computational Electrodynamics The Finite-Differences Time Domain Method* (Artech House, Boston, 2005).
- [19] I. M. Besieris and A. M. Shaarawi, Hopf-Rañada linked and knotted light beam solution viewed as a null electromagnetic field, *Opt. Lett.* **34**, 3887 (2009).
- [20] M. Arrayás and J. L. Trueba, Exchange of helicity in a knotted electromagnetic field, *Ann. Phys. (NY)* **524**, 71 (2012).
- [21] M. Arrayás, A. F. Rañada, A. Tiemblo, and J. L. Trueba, Null electromagnetic fields from dilatation and rotation transformations of the hopfion, *Symmetry* **11**, 1105 (2019).
- [22] M. Arrayás, D. Bouwmeester, and J. L. Trueba, Knots in electromagnetism, *Phys. Rep.* **667**, 1 (2017).
- [23] R. C. David J. Griffiths, *Introduction to Electrodynamics* (Prentice Hall, Englewood Cliffs, NJ, 1999).
- [24] J.-P. Berenger, A perfectly matched layer for the absorption of electromagnetic waves, *J. Comput. Phys.* **114**, 185 (1994).
- [25] S. D. Gedney, An anisotropic perfectly matched layer-absorbing medium for the truncation of FDTD lattices, *IEEE Trans. Antennas Propag.* **44**, 1630 (1996).